Fracture analysis of a corner crack in a pinhole of a solid cylinder under torsion loading

Richardson P. Joseph[a,b], Ichsan Setya Putra[c,d], Agung Setyo Darmawan[e], Haw Ling Liew[f], Singh Ramesh[f,g], Purwo Kadarno[c], Md Asri Mohammad[g] and Judha Purbolaksono[c*]

[a]School of Civil Engineering, Qingdao University of Technology, Qingdao 266033, People Republic of China
[b]Centre for Infrastructure Engineering, Western Sydney University, Penrith, NSW 2571, Australia
[c]Department of Mechanical Engineering, Faculty of Industrial Technology, Universitas Pertamina, Jakarta 12220, Indonesia
[d]Department of Aeronautics and Astronautics, Institut Teknologi Bandung, Bandung 40132, Indonesia
[e]Department of Mechanical Engineering, Faculty of Engineering, Universitas Muhammadiyah Surakarta, Surakarta 57162, Indonesia
[f]Department of Mechanical Engineering, Faculty of Engineering, University of Malaya, Kuala Lumpur 50603, Malaysia
[g]Department of Mechanical Engineering, Faculty of Engineering, Universiti Teknologi Brunei, Gadong BE1410, Brunei

ARTICLE INFO	ABSTRACT
	Fatigue crack growths of a corner crack emanating from a pinhole of a solid cylinder subjected to cyclic torsion loading were simulated using a Dual-Boundary Element Method (DBEM) based software. For a given crack aspect ratio a/c, larger Mode I stress intensity factor (SIF) was observed at a larger pinhole diameter. Any given initial crack aspect ratio a/c would evolve towards unity. The final evolving crack aspect ratio a/c was shown to be larger than 1. For the same given initial crack length a, a smaller crack depth c was found to result in a shorter fatigue life. A shorter fatigue life yielded a larger orientation angle of the crack growth path.

1. Introduction

The cylindrical bars are widely used in engineering applications for machine components and structures. Surface cracks or flaws are frequently initiated in these components due to cyclic applied loads, material defects and improper manufacturing processes. During service loading, the crack or flaw grows into a critical stage, which can then result in an undesirable failure. To ensure the safety of the component to be fit in service, scheduled inspections shall be performed. Thus, understanding of the fatigue crack behavior in components is essential. Machinery components such as turbines, electric motors, power transmissions, etc. commonly have cylindrical parts. In services, those components are often subjected to cyclic torsion loading. Sharp edge, pinhole, notch, slot or keyway in solid cylinders can potentially lead to stress concentration and promote a defect. Some inherent micro cracks in structures are unavoidable as a result of metallurgical defects, manufacturing processes or service handling. When a component has a micro crack and its stress intensity factor is greater than the threshold value of the material fracture toughness, the crack will propagate to become a macro crack.

Various works on fracture analyses using different methods, materials and geometries have been reported by researchers (Alshoaibi, 2020; Abd-Elhady 2013, Abd-Elhady 2020, Aliha & Ayatollahi 2008, 2010; Aliha & Ayatollahi, 2012; Aliha & Ayatollahi 2013; Citarella *et al*., 2014; Predan *et al*., 2013; Zakavi *et al.,* 2019). In particular, fatigue crack growths of a surface crack in a smooth round bar have been reported in literature (Carpinteri & Brighenti, 1996; Carpinteri & Vantadori, 2009; Couroneau & Royer, 1998; Lin & Smith, 1997; Lin & Smith, 1998; Thompson & Sheppard, 1992; Toribio *et al*., 2009; Toribio *et al*., 2011; Toribio *et al*., 2014). Although many works for notched and smooth shafts have been done, only a few fatigue crack growth analyses on a round solid bar with a transverse hole are available in literature. Comprehensive work on life estimations of crack initiation in solid cylinders under multiaxial in-phase and out-of-phase loadings was reported by Jen and Wang (2005). Next, Yip and Jen (1996) reported fatigue life of crack initiation in transverse circular holes of a solid cylinder under combined axial and torsion loading. Joseph *et al*. (2014) presented the fatigue crack growths of a corner in a pinhole subjected to cyclic tension. It simply indicates that numerical methods were often used for evaluating the local stress and strain at components with a geometrical discontinuity.

Considering many mechanical components in services being subjected to torsion loading, the updates on the phenomena of fracture behaviors are always desired. In this work, the stress intensity factors (SIFs) and fatigue crack growths of a corner crack emanating from a pinhole of a solid cylinder under cyclic torsion loading are presented. A numerical analysis is often sought to reduce the experimental works that usually have the complex setup. Here, all the analyses are carried out by using the dual-boundary element software package of BEASY (2014). The BEASY software uses the DBEM which was developed by Mi and Aliabadi (1992) and Cisilino and Aliabadi (1999) for treating the crack boundaries and extensions during the crack growth. The generalized NASGRO equation and the mechanical and fatigue properties of 6061-T6 aluminum alloy (BEASY 2014) are used in this study. A quarter-elliptical corner crack for different crack orientations is introduced at the edge of the pinhole. Effects of the initial crack aspect ratio on the SIFs are studied.

2. Materials and Method

The schematic illustrations of the cracked models are presented in Fig. 1. The schematic model of a semi-elliptical crack in a smooth solid cylinder is shown in Fig. 1a. Figure 1b shows a schematic model of a quarter-elliptical corner crack emanating from a pinhole of a solid cylinder. In modeling, all the surfaces of cylinder region are defined to be in outward normal direction. Two-dimensional quadratic elements were used to discretize all the non-cracked surfaces. A maximum shear stress τ_s of 100 MPa (M_t = 530 x 10^3 N.mm) was used in all cases for calculating the SIFs. The *J*-integral method is used to evaluate the stress intensity factors. The pinhole diameter $\emptyset$ of 6 mm in 30 mm-diameter cylinder was considered for crack growth analyses. Figures 1c-d show the details of the notations used in a semi-elliptical crack and a corner crack. Table 1 lists the mechanical and fracture properties of 6061-T6 aluminum alloy that are used in the NASGRO equation. The minimum strain energy density criterion for crack extension is adopted in BEASY (2014). The modeling strategy of three-dimensional crack problems may be summarized as follows (Mi & Aliabadi, 1992; Cisilino & Aliabadi, 1999):

- Crack surfaces are modeled with discontinuous elements.

- Surfaces intersecting a crack surface are modeled with edge discontinuous quadrilateral or triangular elements.

- The displacement integral equation is applied for collocation on one of the crack surfaces, i.e. the upper surface.

- The traction integral equation is applied for collocation on the opposite crack surface, i.e. the lower surface.

3. Results and Discussion

Prior to introducing an initial crack, the model of a solid cylinder with a pinhole shall be first established. The principal stresses around the pinhole of the twisted shaft are shown in Fig. 2(a). The maximum and minimum principal stresses are shown, respectively, at 45° (225°) and 135° (315°) of the pinhole perimeter. The wireframe initial meshing of a corner crack model is shown in Fig. 2(b).
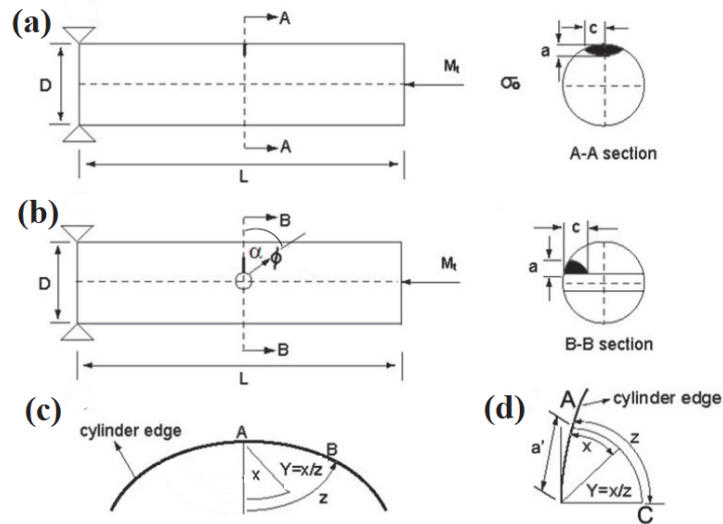
Fig. 1. Schematic diagrams: (a) a semi-elliptical crack in solid cylinder; (b) a corner crack emanating from a pinhole in a solid cylinder; (c) details of the notations used in a semi-elliptical crack; (d) details of the notations used in a corner crack.
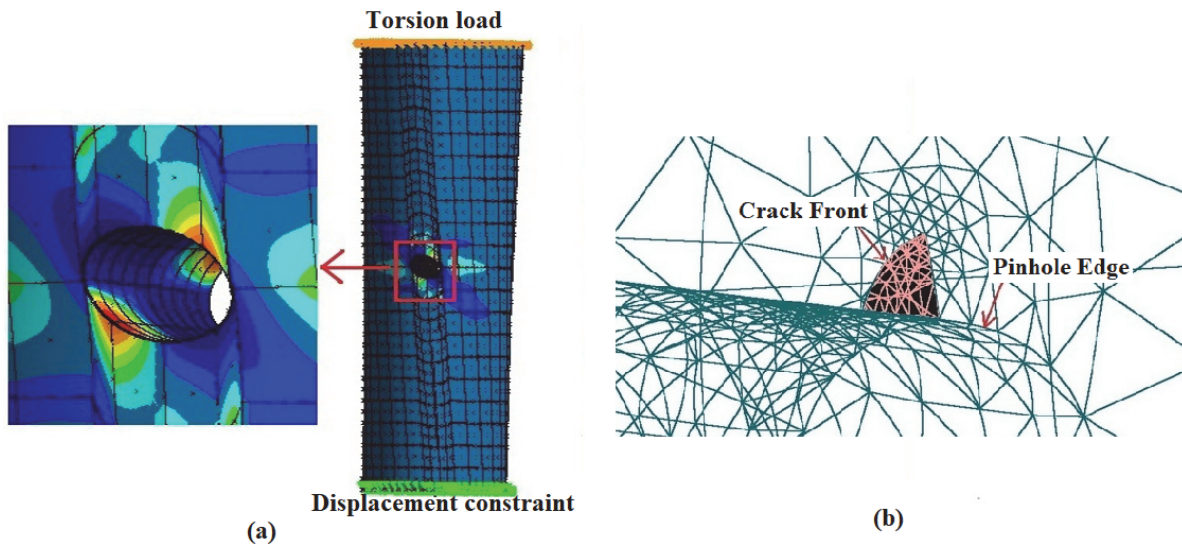
Fig. 2. (a) Twisted shaft with a pinhole and its principal stresses; (b) Wireframe initial meshing of a corner crack model.

To demonstrate the accuracy of the results obtained by using BEASY (2014), the SIFs for a semi-elliptical surface crack in a smooth round bar (Fig. 1a) are validated with the Finite Element Analysis (FEA) results reported by Ismail *et al.* (2012). The 50 mm-diameter smooth round bar with $c/D = 0.1$ is used as the validation model. The normalized stress intensity factors K_{II}/K_o and K_{III}/K_o along the crack front are presented in Fig. 3. The K_o value in all cases is defined as

Table 1. Mechanical and fracture properties of 6061-T6 Aluminum alloy (BEASY 2014)

|	
Modulus of elasticity (GPa)	69
Poisson's ratio	0.33
Yield stress (0.2%) (MPa)	282.69
Ultimate Tensile strength (MPa)	310.26
Plane stress Fracture Toughness, K_C (MPa√mm)	1250.95
Plane Strain Fracture Toughness, K_{IC} (MPa√mm)	903.46
Crack Growth Rate Coefficient (C)	6.53E-10
N coefficient (N)	2.3
P coefficient (P)	0.5
Q coefficient (Q)	0.5
Threshold SIF at $R = 0$ (ΔK_{th}) (MPa√mm)	121.62
Plane stress/strain constraint factor, α	2.0
S_{max}/S_0	0.3

$$K_o = \tau_s \sqrt{\pi c}, \tag{1}$$

where τ_s is the applied maximum shear stress and c is the crack length. Both the solutions, except at $Y = 0.8$, are shown to be in good agreements. It is widely known that the FEA has an inaccuracy of calculating the SIFs at the crack front near the surface intersecting the crack surface (Y is approaching 1) of having corner point singularities. Pook (1994) raised the implication of singularities in the vicinity of a corner point where a crack front intersects a free surface. The consideration of corner point singularities may be necessary for the situations that promote mixed mode loadings, particularly for analyzing mixed mode fatigue crack growths. It is reported that stresses in the vicinity of a corner point are known to be the combined stresses due to two different singularities of different orders: stress intensity factors and corner point singularities (Pook et al., 2015; Pook et al., 2017; Berto et al., 2017). The phenomenon of corner point singularities at the cracked bodies was also reported in later works by Aliha et al. (2015, 2017, 2018, 2019), Pour et al. (2018), Aliha and Bahmani (2017) and Bahmani et al. (2017, 2020). Meanwhile, the DBEM uses the edge discontinuous quadrilateral or triangular elements to treat the singularities at the intersecting surface, resulting in more accurate results (Mi & Aliabadi, 1992; Cisilino & Aliabadi, 1999). At the initial increment, the K_I, K_{II}, K_{III}, and K_{eff} values of a corner crack ($\alpha = 45°$) in a 6 mm-pinhole diameter of a 30 mm-diameter cylinder for different crack aspect ratio a/c are presented in Fig. 4. It can be seen from Fig. 4a that the K_I values at the cylinder edge are shown to increase as the crack aspect ratio a/c decreases. It indicates that, in respect to the crack geometry on K_I, the shorter section of a or c would lead to a larger local normal stress. The K_I values along the crack front for $a/c = 0.67$ are shown to be nearly constant. The K_I value for a/c around 0.67 may be the turning point to be the lowest SIF at the pinhole edge.
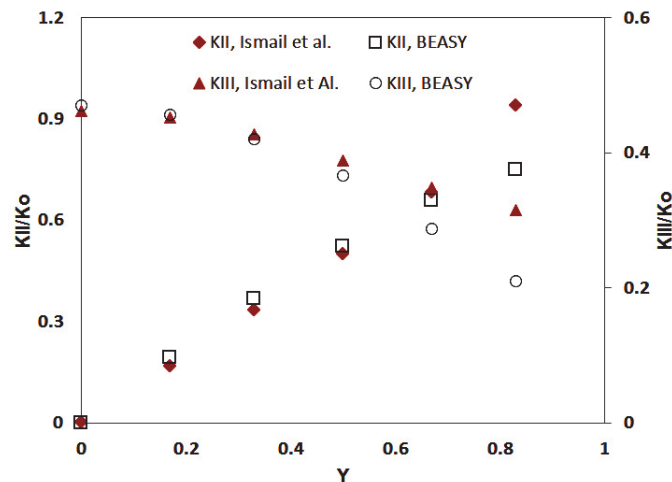
Fig. 3. Comparison of the K_{II} and K_{III} values obtained by using BEASY and those by Ismail *et al.* (2012)

At the crack orientation $\alpha = 45°$ and for a given aspect ratio a/c, the absolute K_{II} values at the pinhole edge (Fig. 4b) are observed to be larger than those at the cylinder edge. In respect to the crack geometry on K_{II}, the shorter section of a or c would lead to a larger local shear stress. In contrast to the K_{II} values, the K_{III} values at the pinhole edge (Fig. 4c) are generally shown to be smaller than those at the cylinder edge. A crack aspect ratio smaller than 0.67 seems to trigger a larger K_{III} values. However, the location of the largest SIF at the crack front varies and depends on the crack aspect ratio a/c. The K_{eff} values along the crack fronts are shown in Fig. 4d. The K_{eff} is defined as $K_{eff} = [(K_I + |K_{III}|)^2 + 2K_{II}^2]^{0.5}$. The patterns of the K_{eff} values along the crack front (Fig. 4d) are shown to be similar to those of K_I values (Fig. 4a). The SIFs for Mode I are observed to contribute dominantly to the K_{eff} values. It can also be evidenced by the magnitudes of the K_I in comparison to those of K_{II} and K_{III}.

It is necessary to evaluate the effect of the crack orientation α (see Fig. 1b) on the SIFs. To demonstrate this purpose, a corner crack ($a/c = 1 = 0.5$ mm/0.5 mm) in a 6 mm-pinhole diameter of a 30 mm-diameter cylinder is used, and the corresponding SIF results are presented in Fig. 5. Figure 5a confirms that the largest K_I values are found at $\alpha = 45°$ where the maximum principal stress is known to be at this angle. Meanwhile, the SIFs along the crack front at $\alpha = 0°$ and $90°$ are found to be nearly zero. The K_{II} and K_{III} values are presented in Figs. 5b and 5c, respectively. At $\alpha \neq 45°$, the absolute K_{II} values at the pinhole edge (Fig. 5b) are generally observed to be smaller than those at the cylinder edge. At $\alpha = 22.5°$, the K_{II} values toward the pinhole edge are found to be asymptotically descending to zero. The maximum absolute K_{III} values (Fig. 5c) are found at the crack front away from the cylinder and pinhole edges. Again, the patterns of the K_{eff} values (Fig. 5d) are shown to be similar to those of the SIFs for Mode I (Fig. 5a). It means that at $\alpha \neq 0°$ and $90°$, the K_I values are the dominant magnitudes in determining the effective stress intensity factors.
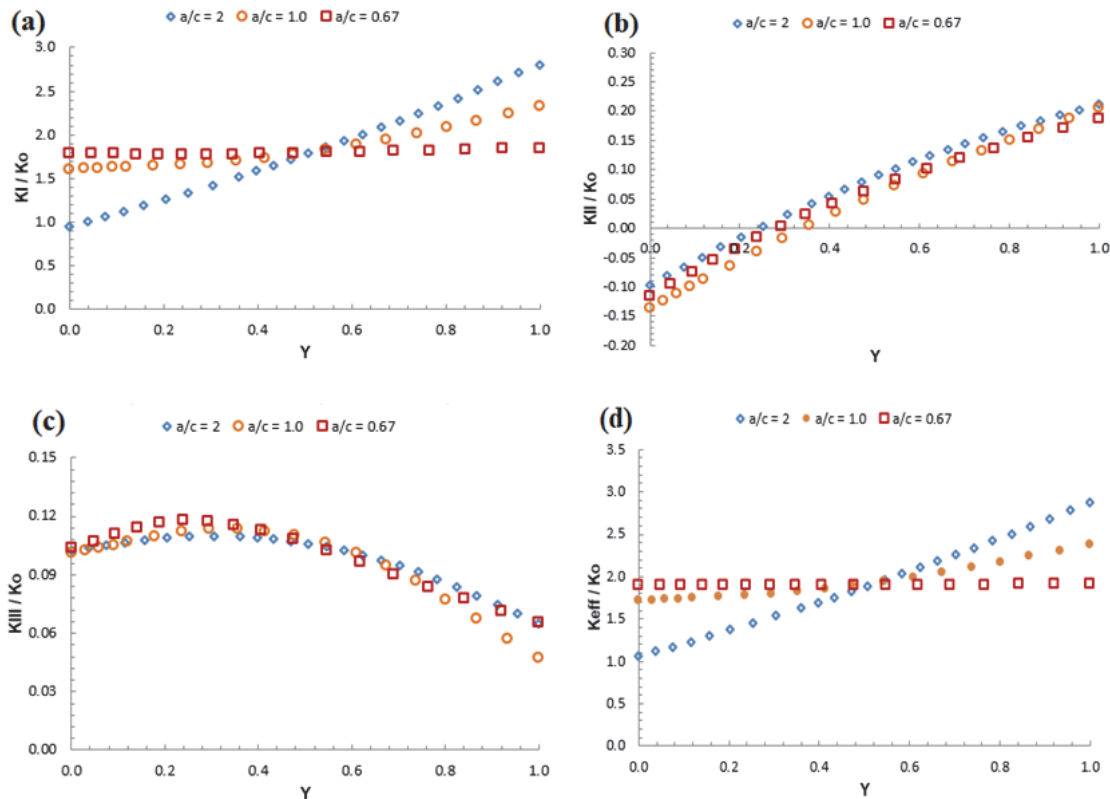
Fig. 4. Normalized SIFs of a corner crack in 6 mm-diameter pinhole of 30 mm-diameter cylinder at $\alpha = 45°$ ($K_0 = \tau_s (\pi. 0.5)^{0.5}$; $a/c = 2 = 1.0/0.5$ (mm/mm); $a/c = 1 = 0.5/0.5$ (mm/mm); $a/c = 0.67 = 0.33/0.5$ (mm/mm): (a) K_I; (b) K_{II}; (c) K_{III}; (d) K_{eff}.
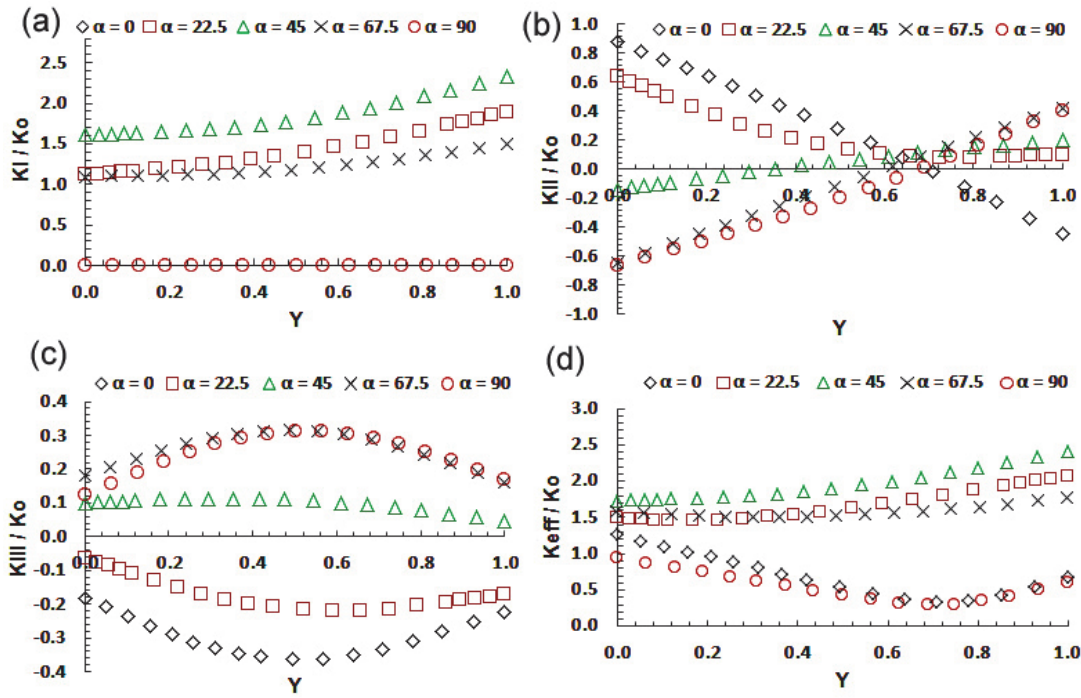
Fig. 5. Effect of crack orientation α on normalized SIFs of a corner crack ($a/c = 1 = 0.5/0.5$) in 6 mm-diameter pinhole of 30 mm-diameter cylinder: (a) K_I; (b) K_{II}; (c) K_{III}; (d) K_{eff}.

Table 2. Normalized stress intensity factors K_I with $K_0 = \tau_s (\pi . 0.5)^{0.5}$

Ø	α	Location	a/c		
			2 (= 1/0.5)	1 (= 0.5/0.5)	0.67 (= 0.33/0.5)
4	0	C	-0.004	-0.001	-0.011
		A	-0.014	-0.007	-0.040
	22.5	C	1.934	1.661	1.339
		A	0.544	0.967	1.119
	45	C	2.626	2.199	1.757
		A	0.792	1.339	1.535
	67.5	C	1.770	1.470	1.188
		A	0.585	0.941	1.055
	90	C	0.005	0.000	0.000
		A	0.037	0.001	0.000
8	0	C	-0.001	-0.004	-0.012
		A	-0.017	-0.003	-0.034
	22.5	C	2.363	1.982	1.608
		A	0.832	1.367	1.510
	45	C	2.989	2.464	2.284
		A	1.148	1.850	2.061
	67.5	C	1.881	1.528	1.222
		A	0.827	1.219	1.308
	90	C	0.000	0.000	0.000
		A	0.000	0.000	0.000

More Mode I SIFs for different pinhole diameters, crack orientation α, and crack aspect ratios a/c are presented in Table 2. Table 2 generally shows that for a given crack aspect ratio a/c, a larger K_I value

are observed at the larger pinhole diameter. It is also confirmed that the larger Mode I SIFs are found at $\alpha = 45°$.

To perform fatigue crack growth analyses, the generalized NASGRO equation that is widely used in many practical analyses is used in this study. The NASGRO equation is written as (Forman et al., 1994):

$$\frac{da}{dN} = \frac{C\ (1-f)^n\ \Delta K^n (1-\frac{\Delta K_{th}}{\Delta K})^p}{(1-R)^n (1-\frac{\Delta K}{(1-R)\ K_C})^q}, \tag{2}$$

where N is the fatigue cycles, a is the crack length (crack depth), R is the stress ratio, ΔK_{th} is the threshold stress intensity factor range, ΔK is the range of stress intensity factors, K_C is the plane stress fracture toughness, and the constants C, n, p, and q are the NASGRO coefficients, and f is the crack opening function that is defined as (Forman et al., 1994):

$$f = Max(R, A_0 + A_1 R + A_2 R^2 + A_3 R^3) \tag{3}$$

for $R \geq 0$, and

$$f = A_0 + A_1 R \tag{4}$$

for $-2 \leq R < 0$. The polynomial coefficients are defined as (Forman et al., 1994):

$$A_0 = (0.825 - 0.34\ \alpha + 0.05\ \alpha^2)\ (\cos[\pi/2.(S_{mas}/S_0)])^{1/\alpha}, \tag{5}$$

$$A_1 = (0.415 - 0.071\ \alpha).S_{max}/S_0, \tag{6}$$

$$A_2 = 1 - A_0 - A_1 - A_3, \tag{7}$$

$$A_3 = 2A_0 + A_1 - 1, \tag{8}$$

where α is the plane stress/strain constraint factor, and S_{max}/S_0 is the ratio of the peak stress to the material flow stress in a stress cycle. The constants α and S_{max}/S_0 are available as the fitting constants (BEASY 2014).

To validate the estimations obtained by using BEASY (2014), the fatigue growth with a constant stress ratio $R = 0.1$ of a surface crack ($a = 0.5$ mm and $c = 0.5$ mm) in a 15.9 mm-diameter smooth cylinder is compared with the experimental result reported by Thompson and Sheppard (1992) as presented in Fig. 6. The cylinder that is made of Al 2024-T351 is subjected to a maximum cyclic torsion loading of 134.28 MPa. At the stable stage, even though having a similar slope of the curve, the estimation done by using BEASY (2014) shows more conservative than that by Thompson and Sheppard (1992). Very good agreement is shown for the estimation at the unstable stage. However, this is desirable in the preliminary engineering design process.

Fatigue growths of a corner crack at $\alpha = 45°$ for different crack aspect ratios a/c emanating from a 6 mm-diameter pinhole of a 30 mm-diameter solid cylinder under a constant amplitude load of $R = 0$ (a maximum shear stress of 265 MPa or $M_t = 1.4 \times 10^6$ N.mm) are presented in Fig. 7. The crack lengths c ($= c_0 + \Delta c$) and a' ($= a'_0 + \Delta a'$) are, respectively, measured at the pinhole and cylinder edges (see Fig. 1), where c_0 and a'_0 are the initial crack length and depth, and Δc and $\Delta a'$ are the crack increments. In all cases, initially, the faster crack growth is found at the pinhole. Next, after the evolving crack aspect ratio a/c be around 1, the crack growths at the cylinder edge are observed to be faster than those at the pinhole edge. It leads to the final evolving crack aspect ratio a/c to be larger than 1. It can also be seen from Fig. 7, for the same given initial crack length a, a smaller crack depth c was found to lead to a shorter fatigue life. It may be due to the fact that the shorter crack length at the pinhole edge has a larger K_I value,

causing a larger opening mode. Meanwhile, for the same initial crack depth c, different crack lengths comparatively result in similar fatigue lives.
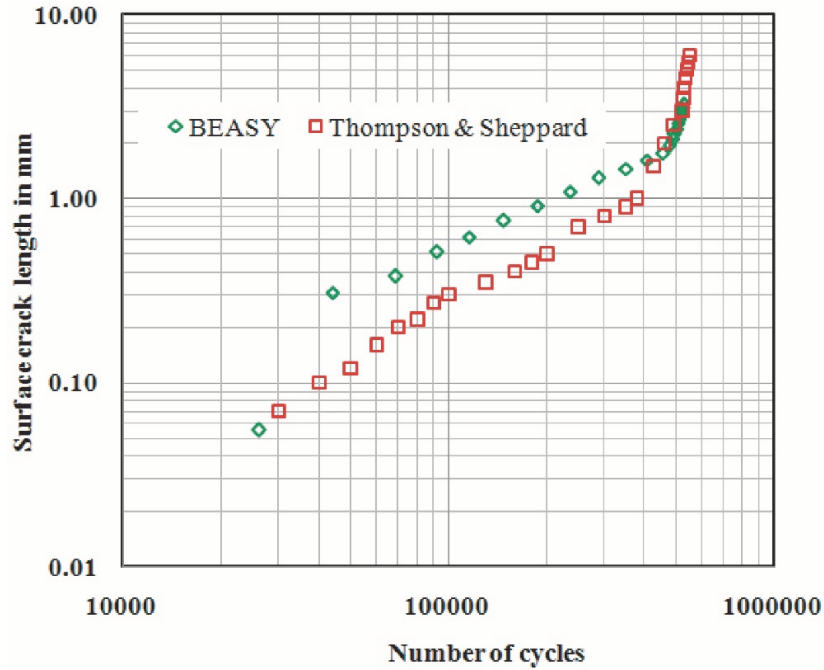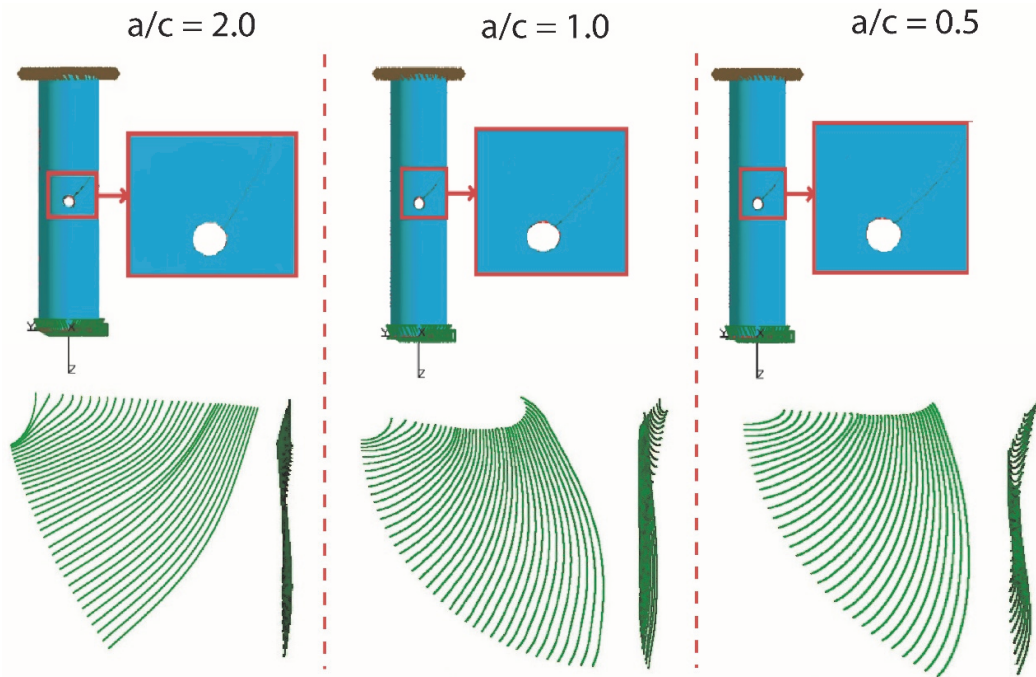

Fig. 6. Fatigue crack growths under cyclic torsion by Thompson and Sheppard (1992) (experimental work) and present work with NASGRO equation
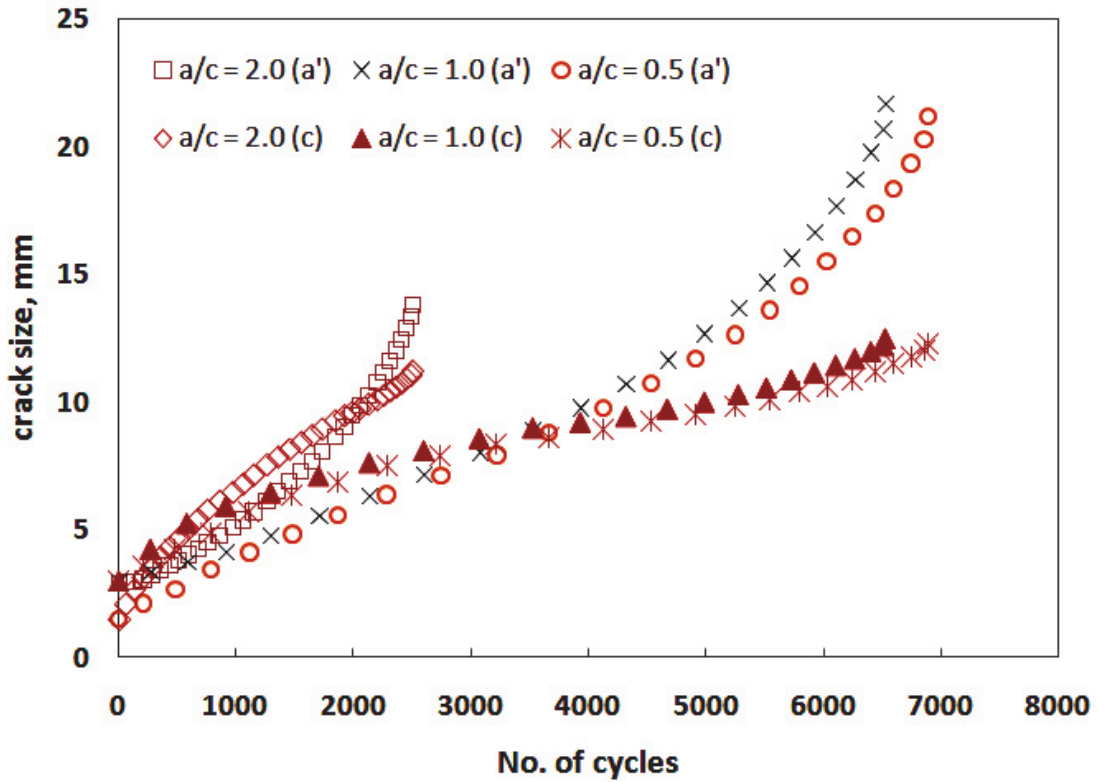
Fig.7. Effect of the initial crack aspect ratio ($a/c = 2 = 3.0/1.5$; $a/c = 1 = 3.0/3.0$; $a/c = 0.5 = 1.5/3.0$) on the fatigue life under constant amplitude loading ($R = 0$)

Fig. 8. Crack paths (top) and crack shape evolutions (bottom) during the fatigue crack growth for different crack aspect ratios (initial $\alpha = 45°$, $a/c = 2 = 3.0/1.5$ mm/mm; $a/c = 1 = 3.0/3.0$ mm/mm; $a/c = 0.5 = 1.5/3.0$ mm/mm) under constant amplitude loading ($R = 0$)

Fig. 8 shows the crack path and crack shape evolutions of a corner crack for different crack aspect ratios. The crack planes are shown to be waved and twisted during the crack growths. This is as a result of the changes of the principal stress distribution around the crack front. It can also be from Fig. 8 that a shorter fatigue life tends to yield a larger α of the crack path.

4. Conclusions

Stress intensity factors and fatigue crack growths of a corner crack emanating from pinhole of a cylinder under torsion loading were presented. Some concluding remarks may be fairly drawn as follows:

- For given crack aspect ratio a/c, larger Mode I SIFs were observed at a larger pinhole diameter.
- At $\alpha = 45°$ and for a given aspect ratio a/c, the absolute K_{II} values at the pinhole were observed to be larger than those at the cylinder edge. Meanwhile, the K_{III} values at the pinhole edge were generally found to be smaller than those at the cylinder edge.
- For given crack aspect ratios, the crack growth at the pinhole edge was initially found to be faster than that at the cylinder edge. Then, after the crack aspect ratio a/c approached a unity, the crack growths at the cylinder edge were observed to be faster than those at the pinhole edge, leading to the final evolving crack aspect ratio a/c to be larger than 1.
- For the same given crack length a, a smaller crack depth c resulted in a shorter fatigue life.
- A shorter fatigue life produced a larger evolving angle α of the crack path.

Acknowledgments

References

Abd-Elhady, A. (2013). Mixed mode I/II stress intensity factors through the thickness of disc type specimens. *Engineering Solid Mechanics, 1*(4), 119-128.

Alshoaibi, A. (2020). Finite element-based model for crack propagation in linear elastic materials. *Engineering Solid Mechanics, 8*, 131-142.

Aliha, M.R.M. & Ayatollahi, M. R. (2008). On mixed-mode I/II crack growth in dental resin materials. *Scripta Materialia, 59*(2), 258-261.

Aliha, M.R.M., Ayatollahi, M. R., Smith, D.J. & Pavier, M. J. (2010). Geometry and size effects on fracture trajectory in a limestone rock under mixed mode loading. *Engineering Fracture Mechanics, 77*(11), 2200-2212.

Aliha, M.R.M. & Ayatollahi, M. R. (2012). Analysis of fracture initiation angle in some cracked ceramics using the generalized maximum tangential stress criterion. *International Journal of Solids and Structures, 49*(13), 1877-1883.

Aliha, M. R. M., Bahmani, A., & Akhondi, S. (2015). Numerical analysis of a new mixed mode I/III fracture test specimen. *Engineering Fracture Mechanics, 134*, 95-110.

Aliha, M.R.M. & Saghafi, H. (2013). The effects of thickness and Poisson's ratio on 3D mixed-mode fracture. *Engineering Fracture Mechanics, 98*, 15-28.

Aliha, M. R. M., & Bahmani, A. (2017). Rock fracture toughness study under mixed mode I/III loading. *Rock Mechanics and Rock Engineering, 50*(7), 1739-1751.

Aliha, M. R. M., Linul, E., Bahmani, A., & Marsavina, L. (2018). Experimental and theoretical fracture toughness investigation of PUR foams under mixed mode I+ III loading. *Polymer Testing, 67*, 75-83.

Aliha, M.R.M., Shaker, S. & Keymanesh, M.R. (2019). Low temperature fracture toughness study for bitumen under mixed mode I + II loading condition. *Engineering Fracture Mechanics, 206*, 297-309.

Bahmani, A., Aliha, M. R. M., & Berto, F. (2017). Investigation of fracture toughness for a polycrystalline graphite under combined tensile-tear deformation. *Theoretical and Applied Fracture Mechanics, 90*, 53-64.

Bahmani, A., Aliha, M.R.M., Jebalbarezi Sarbijan, M. & Mousavi, S.S. (2020). An extended edge-notched disc bend (ENDB) specimen for mixed-mode I+II fracture assessments. *International Journal of Solids and Structures*, *193–194*, 239-250.

BEASY, Release 14 (2014). BEASY Ashurst Lodge, Ashurst, Southampton SO40 7AA, United Kingdom, http://www.beasy.com

Berto, F., Pook, L., & Campagnolo, A. (2017). Corner point singularities under in-plane and out-of-plane loading: a review of recent results. *Engineering Solid Mechanics, 5*(3), 167-176.

Carpinteri, A. & Brighenti, R. (1996). Fatigue propagation of surface flaws in round bars: a three-parameter theoretical model. *Fatigue & Fracture of Engineering Materials and Structures*, *19*, 1470-1480.

Carpinteri, A. & Vantadori, S. (2009). Sickle-shaped cracks in metallic round bars under cyclic eccentric axial loading. *International Journal of Fatigue*, *31*, 759-765.

Cisilino, A.P. & Aliabadi, M.H. (1999). Three-dimensional boundary element analysis of fatigue crack growth in linear and non-linear fracture problems. *Engineering Fracture Mechanics*, *63*(6), 713-733.

Citarella, R., Lepore, M., Shlyannikov, V. & Yarullin, R. (2014). Fatigue surface crack growth in cylindrical specimen under combined loading. *Engineering Fracture Mechanics*, *131*, 439-453

Couroneau, N. & Royer, J. (1998). Simplified model for the fatigue growth analysis of surface cracks in round bars under mode I. *International Journal of Fatigue*, *20*, 711-718.

Forman, R.G., Shivakumar, V. & Newman Jr., J.C. (1994), *Fatigue Crack Growth Computer Program NASA/FLAGRO Version 2.0*, National Aeronautics and Space Administration (NASA).

Ismail, A.E., Ariffin, A.K., Abdullah, S. & Ghazali, M.J. (2012). Stress intensity factors for surface cracks in round bar under single and combined loadings. *Meccanica*, *47*(5), 1141-1156.

Jen, Y.-M. & Wang, W.-W. (2005). Crack initiation life prediction for solid cylinders with transverse circular holes under in-phase and out-of-phase multiaxial loading. *International Journal of Fatigue*, *27*(5), 527-539.

Joseph, R.P., Purbolaksono, J., Liew, H.L., Ramesh, S. & Hamdi, M. (2014). Stress intensity factors of a corner crack emanating from a pinhole of a solid cylinder. *Engineering Fracture Mechanics, 128*, 1-7.

Lin, X.B. & Smith, R.A. (1997). Shape growth simulation of surface cracks in tension fatigued round bars. *International Journal of Fatigue, 19*, 461-469.

Lin, X.B. & Smith, R.A. (1998). Fatigue growth simulation for cracks in notched and unnotched round bars. *International Journal of Mechanical Sciences, 40*, 405-419.

Mi, Y. & Aliabadi, M.H. (1992). Dual boundary element method for three-dimensional fracture mechanics analysis. *Engineering Analysis with Boundary Elements*, *10*(2), 161-171.

Predan, J., Močilnik, V. & Gubeljak, N. (2013). Stress intensity factors for circumferential semi-elliptical surface cracks in a hollow cylinder subjected to pure torsion. *Engineering Fracture Mechanics*, *105*, 152-168.

Pook, L.P. (1994). Some implications of corner point singularities. *Engineering Fracture Mechanics*, *48*(3), 367-378.

Pook, L.P., Campagnolo, A., Berto, F. & Lazzarin, P. (2015). Coupled fracture mode of a cracked plate under anti-plane loading. *Engineering Fracture Mechanics*, *134*, 391-403.

Pook, L.P., Berto, F., & Campagnolo, A. (2017). State of the art of corner point singularities under in-plane and out-of-plane loading. *Engineering Fracture Mechanics 174*, 2-9.

Pour, P. H., Aliha, M. R. M., & Keymanesh, M. R. (2018). Evaluating mode I fracture resistance in asphalt mixtures using edge notched disc bend ENDB specimen with different geometrical and environmental conditions. *Engineering Fracture Mechanics, 190*, 245-258.

Thompson, K. & Sheppard, S. (1992). Fatigue crack growth in notched and plain shafts subjected to torsion and axial loading. *Engineering Fracture Mechanics*, *43*, 55-71.

Toribio, J., Matos, J.C., Gonzalez, B. & Escuadra, J. (2009). Numerical modelling of crack shape evolution for surface flaws in round bars under tensile loading. *Engineering Failure Analysis*, 16, 618-630.

Toribio, J., Matos, J.C., Gonzalez, B. & Escuadra, J. (2011). Compliance evolution in round cracked bars under tensile fatigue. *Engineering Fracture Mechanics*, *78*, 3243-3252.

Toribio, J., Matos, J.C., Gonzalez, B. & Escuadra, J. (2014). Numerical modelling of cracking path in round bars subjected to cyclic tension and bending. *International Journal of Fatigue*, *58*, 20-27.

Yip, M.-C. & Jen, Y.-M. (1996). Biaxial fatigue crack initiation life prediction of solid cylindrical specimens with transverse circular holes. *International Journal of Fatigue*, *18*(2), 111-117.

Zakavi, B., Kotousov, A., Khanna, A. & Branco, R. (2019). A new method for analysis of part-elliptical surface cracks in structures subjected to fatigue loading. *Theoretical and Applied Fracture Mechanics*, *103*, 102258.